Society of Medical Education & Research

2025, Volume 5, Issue 2, Page No: 78-97
ISSN: 3108-4834

Archive of International Journal of Cancer and Allied Science

Cysteine Dioxygenase 1 Suppresses Gastric Cancer Cell Proliferation by Inducing Oxidative and Integrated Stress Responses

Ivan Sergeevich Mikhailov[1]*, Daria Alexandrovna Sorokina[1]

[1]Department of Clinical Oncology, Lomonosov Moscow State University Clinic, Moscow, Russia.

***E-mail** ✉ i.mikhailov.msu@yahoo.com

Abstract

Cysteine dioxygenase 1 (CDO1) is frequently silenced in various cancers, including gastric cancer (GC), due to promoter hypermethylation, yet its functional role and underlying mechanisms remain poorly understood. In this study, we show that low CDO1 expression correlates with poor prognosis in GC patients. Restoration of CDO1 expression in GC cells significantly suppresses cell proliferation both in vitro and in vivo. Mechanistic investigations reveal that CDO1 inhibits proliferation by elevating oxidative stress, thereby activating the integrated stress response (ISR) in GC cells. High-throughput screening of an antioxidant library identifies Engeletin, a flavanonol glycoside, as an agent capable of mitigating oxidative stress and ISR activation, which in turn diminishes the growth-inhibitory effects of CDO1. Furthermore, either genetic disruption or pharmacological inhibition of the ISR enhances proliferation in CDO1-expressing GC cells. These findings elucidate the molecular mechanisms by which CDO1 exerts its cytostatic effects and highlight its role in regulating GC cell proliferation.

Keywords: Oxidative, Gastric cancer, Cancer cell, CDO1

Introduction

Emerging evidence highlights that abnormal regulation of metabolic enzymes significantly contributes to cancer initiation, progression, and metastasis. Among these enzymes, cysteine dioxygenase 1 (CDO1) is frequently downregulated in various cancers, including lung [1], endometrial [2], breast [3], prostate [4], clear-cell renal cell [5], and gastrointestinal malignancies [6]. Loss of CDO1 expression is often associated with worse survival outcomes in patients across these cancer types [4, 5, 7-10]. Beyond its prognostic relevance, CDO1 has potential diagnostic applications; for example, it may aid in detecting minimal residual disease in the peritoneum of patients with gastric cancer (GC) [11, 12]. In 2020, GC ranked fifth in global incidence and fourth in cancer-related mortality [13]. The observed reduction of CDO1 in GC tissues [14] suggests that its loss may facilitate GC development and progression.

Functionally, CDO1 is critical for maintaining intracellular cysteine balance by catalyzing its oxidation to cysteine sulfinic acid (CSA), which can then be metabolized into taurine or sulfate (SO_4^{2-}) through two distinct pathways [15]. In mice, Cdo1 deletion leads to growth retardation and postnatal lethality [15]. These knockout mice display a sharp decrease in taurine levels, accompanied by a modest rise in plasma sulfate compared with heterozygous or wild-type counterparts [15]. Importantly, the sulfur-containing products generated by CDO1 activity may disrupt cellular redox equilibrium, thereby promoting oxidative stress. Recent studies have linked CDO1 to ferroptosis, a regulated form of cell death driven by lipid peroxidation. Specifically, CDO1 facilitates erastin-induced ferroptosis in triple-negative breast cancer cells, whereas silencing CDO1 prevents ferroptosis in GC cells [16, 17]. Moreover, CDO1 loss has been shown to accelerate

Access this article online https://smerpub.com/

Received: 08 April 2025; **Accepted:** 12 September 2025

How to cite this article: Mikhailov IS, Sorokina DA. Cysteine Dioxygenase 1 Suppresses Gastric Cancer Cell Proliferation by Inducing Oxidative and Integrated Stress Responses. Arch Int J Cancer Allied Sci. 2025;5(2):78-97. https://doi.org/10.51847/SgLtaNGDTn

proliferation in non-small cell lung cancer (NSCLC) cells harboring constitutively active NRF2 by reducing the accumulation of toxic sulfite intermediates (SO32−) [18]. Despite these advances, the comprehensive mechanisms by which CDO1 suppresses malignant traits remain largely undefined.

In this work, we confirm that CDO1 is downregulated in GC tissues and serves as an independent prognostic indicator. Using both cellular and animal models, we demonstrate that restoring CDO1 expression significantly restrains GC cell proliferation. Mechanistically, CDO1 induces oxidative stress, leading to mitochondrial dysfunction and subsequent activation of the integrated stress response (ISR). Collectively, our findings elucidate the molecular basis through which CDO1 exerts its antiproliferative effects in GC.

Results and Discussion

Low CDO1 expression predicts poor outcomes in gastric cancer

To clarify the involvement of CDO1 in gastric cancer (GC), we assessed its expression in patient tumor tissues and matched adjacent normal tissues. Quantitative analysis revealed a pronounced reduction of CDO1 mRNA in GC samples compared to adjacent non-cancerous tissues ($N = 30$, $p < 0.001$), consistent with previous observations from the GSE29272 microarray dataset in the Gene Expression Omnibus **(Figures 1a and b).** At the protein level, immunohistochemistry (IHC) showed that strong CDO1 staining was present in approximately 65% of normal samples, whereas only around 30% of GC samples exhibited similar intensity ($N = 130$, $p < 0.001$) (**Figures 1c and 1d**, **Table 1**). Analysis of clinical parameters indicated that patients with low CDO1 expression had significantly larger tumors, suggesting that diminished CDO1 may facilitate enhanced tumor proliferation ($p = 0.0027$; **Table 2).** Survival evaluation further demonstrated that reduced CDO1 levels were associated with worse overall survival (OS) in GC patients ($N = 130$; median OS: 29 months; $p < 0.001$ high, 45 months vs. low,) (**Figure 1e**). Importantly, multivariate regression analysis identified CDO1 as an independent prognostic factor for favorable OS ($p = 0.028$; **Table 3)**. These findings collectively indicate that loss of CDO1 expression contributes to GC progression and may serve as a valuable prognostic marker.

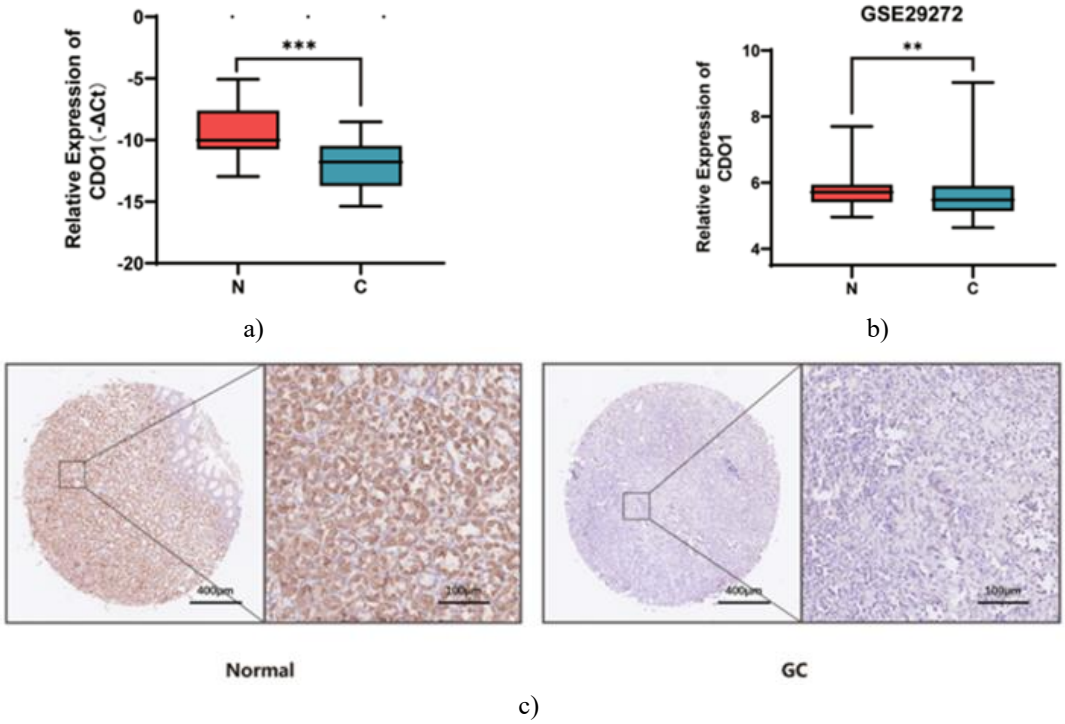

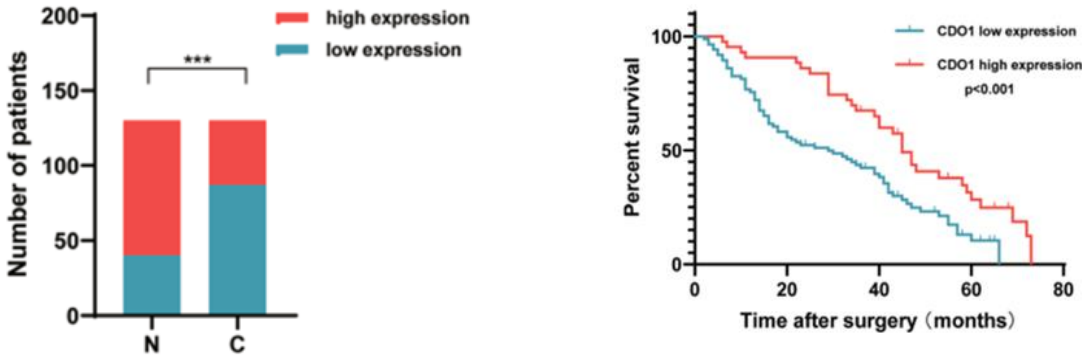

d) e)

Figure 1. Reduced CDO1 expression in Gastric Cancer (GC) tissues is associated with poor prognosis**.**

a. Quantitative analysis of CDO1 mRNA in 30 paired GC and adjacent normal tissues showed a marked decrease in tumor samples compared with normal gastric tissues. **b.** Examination of an independent GC cohort (GSE29272) further confirmed that CDO1 mRNA levels were significantly lower in cancerous tissues than in their normal counterparts. **c.** Immunohistochemical (IHC) staining revealed stronger CDO1 signal in normal gastric mucosa relative to GC tissues. Representative images from one matched pair are presented. Scale bars: 400 μm and 100 μm. **d.** Statistical analysis indicated that roughly 50% of normal tissues exhibited high CDO1 protein expression, whereas only ~20% of GC samples showed similar levels (N = 130). **e.** Kaplan–Meier survival curves demonstrated that GC patients with elevated CDO1 protein levels had better overall survival. Patients were stratified into high and low expression groups based on the median IHC-quantified CDO1 protein level. $^{**}p < 0.01$, $^{***}p < 0.001$.

Table 1. Comparative analysis of CDO1 expression in GC and normal tissues.

	CDO1		*P*-value	χ^2-value
	Low expression	High expression		
Normal	40	90	34.00	<0.001

Table 2. The clinical relevance of CDO1 expression in patients with GC.

Characteristics	CDO1		χ^2-Value	*P*-value
	Low expression	High expression		
Gender				
Female	20	15		
Male	67	28	2.0701	0.1503
Age				
≥60	46	17		
<60	41	26	2.050	0.1522
pT stage				
pT2	7	1		
pT3	4	5	3.5902	0.1661
pT4	76	37		
Tumor location				
Upper third	6	10		
Midle third	9	6	4.4800	0.3450

Lower third	10	7		
More than2/3third All	5	2		
Tumor size				
<6	25	24	8.9841	**0.0027**
≥6	62	19		
pN stage				
pN0	18	11	0.3973	0.5285
pN1-3	69	32		
Lauren type				
Intestinal	67	29	3.7072	0.1567
Diffuse	29	11		
Mixed	1	3		

Pathological T stage (pT), pathological N stage (pN), and overall pathological stage (pTNM) were determined according to the 8th edition of the AJCC Staging System.
Statistically significant P-values are highlighted in bold.

Table 3. Univariate and multivariate analysis evaluating the impact of CDO1 expression on clinical outcomes in gastric cancer patients.

Characteristics	Univariate analysis		Multivariate analysis	
	HR (95%CI)	***P*-value**	**HR (95%CI)**	***P*-value**
pN stage				
pN0 VS pN1-3	1.954(1.156-3.301)	**0.007**	01.533(0.896-2.621)	0.119
Tumor size				
≥6 VS < 6	2.954(1.872-4.660)	**0.001**	2.507(1.570-4.004)	**0.01**
Expression of CDO1				
Low VS High	0.497(0.319-0.772)	**0.002**	0.603(0.384-0.946)	**0.028**
Age				
≥60 VS < 60	1.474(0.996-2.183)	0.052		
pT stage				
pT2 VS pT3-4	1.045(0.456-2.394)	0.917		

CI, confidence interval; HR, hazard ratio
P-values considered statistically are in bold.

CDO1 Suppresses proliferation of gastric cancer cells

Since CDO1 expression was found to be downregulated in GC, we next investigated its role in cell proliferation by introducing either a CDO1-expressing or control lentivirus into MKN45 and NCI-N87 cells. Successful restoration of CDO1 expression was confirmed by immunoblotting (**Figures 2a**). To assess the effect of CDO1 on cell growth, a CCK-8 assay was performed. The results showed that CDO1 markedly reduced the viability of MKN45 and NCI-N87 cells, whereas control cells continued to proliferate over the same time period (**Figures 2b**).

In addition, an EdU incorporation assay was conducted to evaluate DNA replication. The proportion of control MKN45 and NCI-N87 cells in S phase was significantly higher than in cells overexpressing CDO1 (**Figures 2c**). Furthermore, xenograft tumors generated from CDO1-expressing cells were substantially smaller, and the tumor weights were significantly lower compared with those derived from control cells (**Figures 2d and 2e**).

Overall, these results indicate that CDO1 suppresses GC cell proliferation in vitro and inhibits tumor growth in vivo.

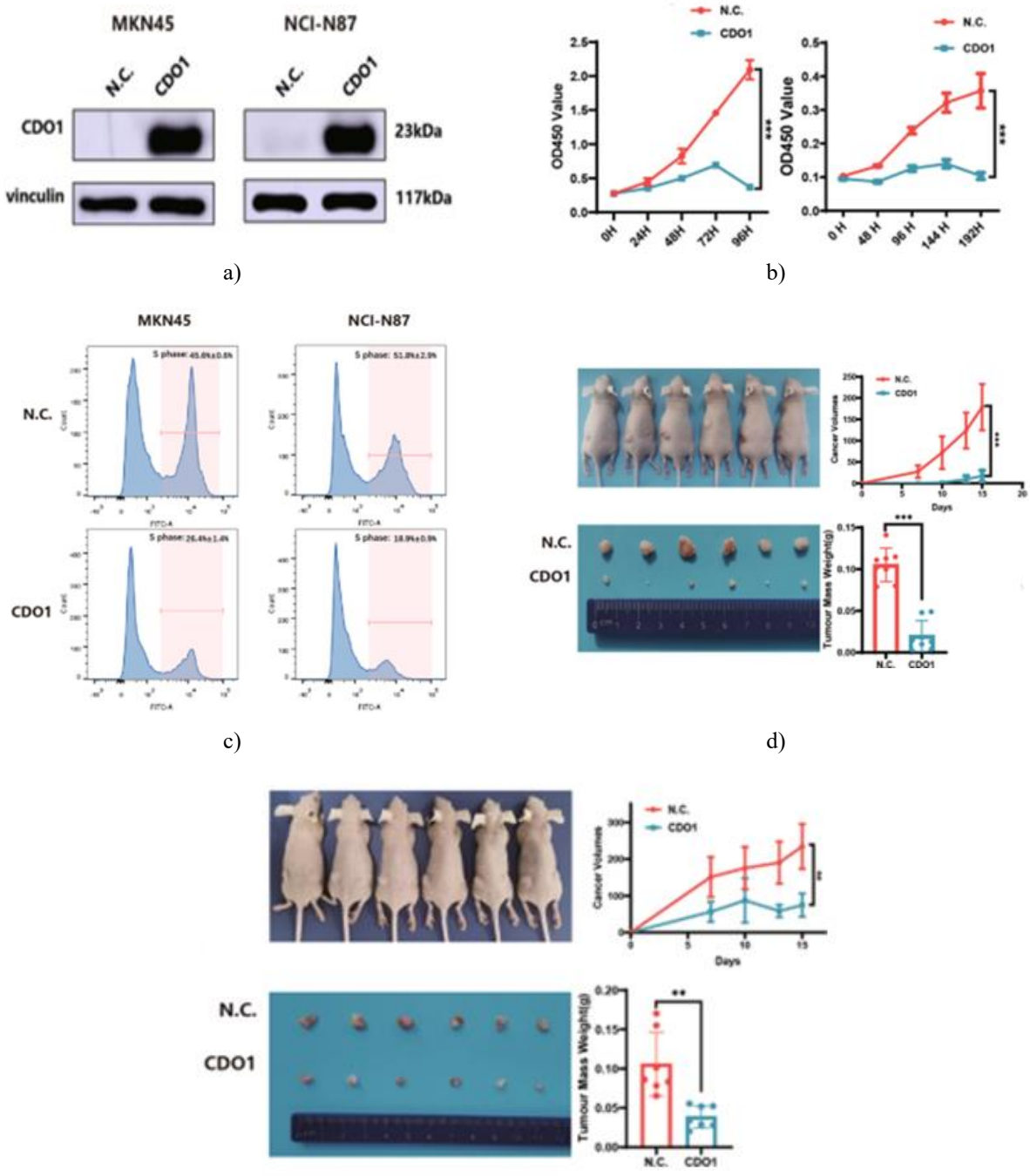

Figure 2. CDO1 suppresses gastric cancer cell proliferation

a. Re-expression of CDO1 in MKN45 (left) and NCI-N87 (right) cells was confirmed by immunoblotting. **b.** CCK-8 assays were used to evaluate the growth of MKN45 (left) and NCI-N87 (right) cells transduced with control (N.C.) or CDO1-expressing lentivirus at the indicated time points (N = 6, mean ± SD). CDO1

restoration significantly reduced the proliferation of both GC cell lines. **c.** EdU staining and flow cytometry analysis of MKN45 (left) and NCI-N87 (right) cells revealed that overexpression of CDO1 markedly decreased the proportion of replicating cells compared with controls. Representative data are shown (N = 3, mean ± SD). **d, e.** In vivo, xenograft tumors derived from MKN45 (d) and NCI-N87 (e) cells in female Balb/c nude mice demonstrated that CDO1 strongly inhibited tumor growth, as evidenced by slower tumor progression over time and reduced tumor weights. **p < 0.01, ***p < 0.001.

The anti-proliferative effect of CDO1 requires its enzymatic activity

To determine whether the inhibitory effect of CDO1 on GC cell proliferation depends on its enzymatic function, we introduced a catalytically inactive mutant, $CDO1^{Y157F}$. Unlike wild-type CDO1, this mutant completely lost its ability to suppress the viability of MKN45 and NCI-N87 cells, as shown by CCK-8 assays (**Figures 3a and b**). Similarly, colony formation assays demonstrated that NCI-N87 cells expressing $CDO1^{Y157F}$ regained their proliferative capacity compared with cells expressing wild-type CDO1 (**Figure 1**). Consistently, in xenograft models, MKN45 cells expressing $CDO1^{Y157F}$ grew comparably to control cells, confirming that the mutated enzyme could not inhibit tumor growth in vivo (**Figures 3c**). These findings indicate that the canonical enzymatic activity of CDO1 is essential for its anti-proliferative function in gastric cancer cells.

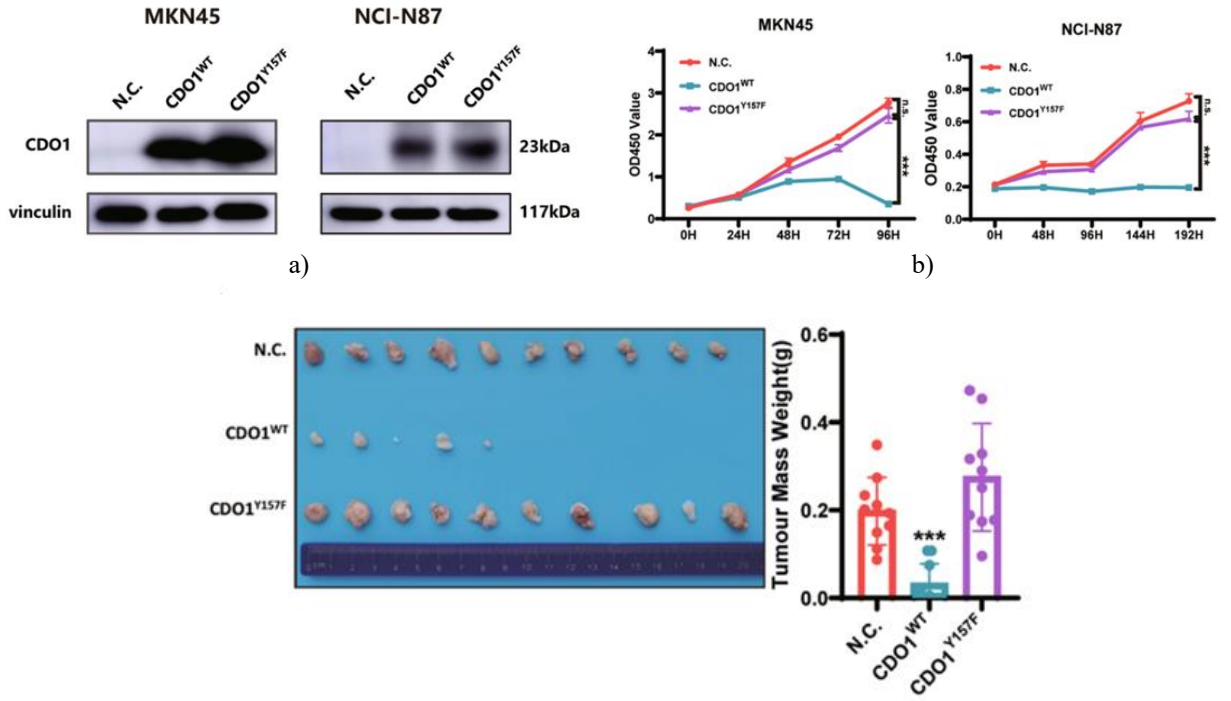

Figure 3. CDO1 Suppresses Proliferation via Its Enzymatic Activity

a. Immunoblotting verified the expression of wild-type CDO1 (CDO1^WT) and the enzymatically inactive mutant ($CDO1^{Y157F}$) in MKN45 (left) and NCI-N87 (right) cells. **b.** Unlike $CDO1^{WT}$, the $CDO1^{Y157F}$ mutant did not reduce the proliferation of MKN45 (left) or NCI-N87 (right) cells in vitro, as assessed by CCK-8 assays at various time points (N = 6, mean ± SD). **C.** In xenograft experiments, $CDO1^{Y157F}$-expressing MKN45 cells showed no suppression of tumor growth. Representative tumor images and weights from the three groups are shown (N = 10 mice per group). ***p < 0.001; n.s., not significant.

CDO1 enhances oxidative stress to inhibit GC cell proliferation

Previous studies indicated that cysteine sulfinic acid (CSA) and sulfite (SO_3^{2-}), metabolic products of CDO1, can impair cell viability in non-small cell lung cancer [18]. To determine whether CDO1 similarly induces oxidative stress in gastric cancer cells, we measured reactive oxygen species (ROS) levels. CDO1 overexpression significantly increased ROS in both MKN45 and NCI-N87 cells (**Figures 4a and 4b**). Additionally, CDO1 reduced intracellular glutathione (GSH) levels while increasing oxidized glutathione (GSSG), leading to a lower GSH/GSSG ratio (**Figures 4c and 4d**). In contrast, the enzymatically inactive $CDO1^{Y157F}$ failed to elevate ROS or alter the GSH/GSSG ratio, highlighting that the enzymatic activity of CDO1 is required for oxidative stress induction in GC cells (**Figures 4a–d**).

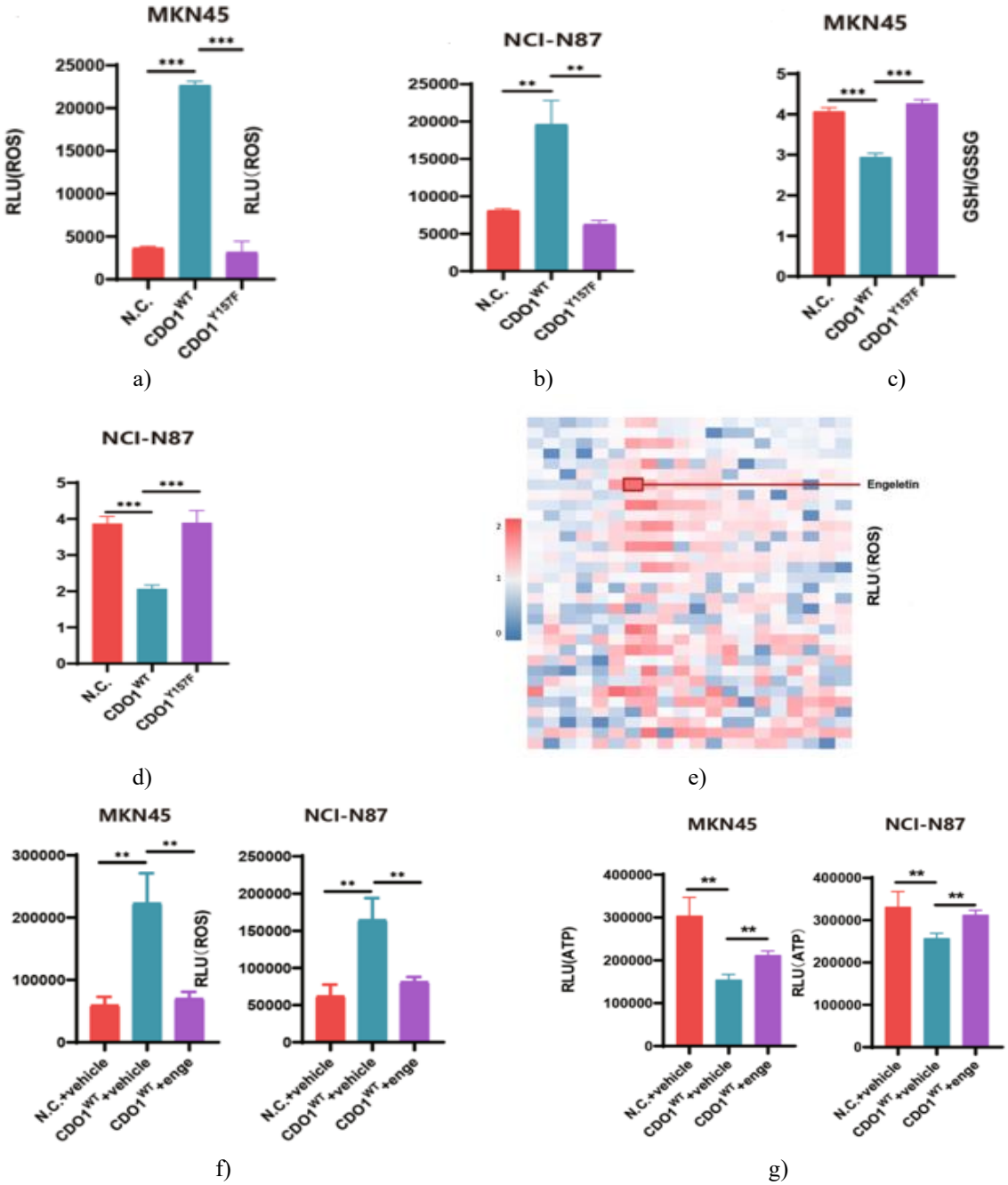

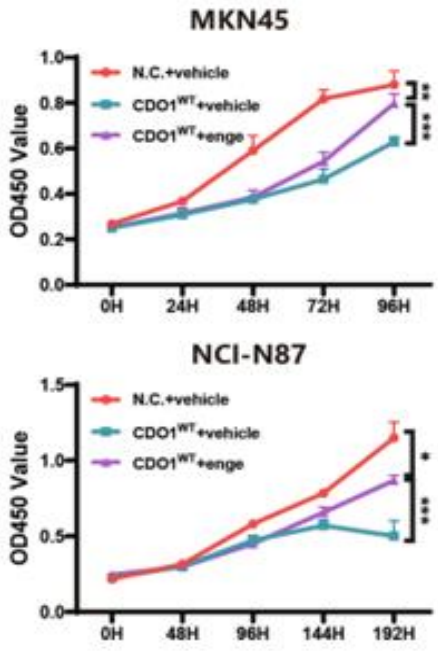

h)

Figure 4. CDO1 promotes oxidative stress in gastric cancer cells

a, b. Overexpression of wild-type CDO1 ($CDO1^{WT}$) significantly elevated ROS levels in MKN45 (A) and NCI-N87 (B) cells, whereas the enzymatically inactive $CDO1^{Y157F}$ had no effect. **c, d.** $CDO1^{WT}$, but not $CDO1^{Y157F}$, decreased the intracellular GSH/GSSG ratio in MKN45 (C) and NCI-N87 (D) cells, indicating a shift toward oxidative stress. **e.** Heatmap illustrating fold changes of antioxidant compounds in high-throughput screening (HTS) relative to vehicle-treated MKN45 cells. Cell viability was assessed via ATP levels measured by CellTiter-Glo, with engeletin-treated MKN45 cells showing approximately a two-fold increase in luminescence. Fold changes were calculated as: Fold change = (Reads (antioxidant) – Reads (Vehicle)) / Reads (Vehicle). **f.** Treatment with engeletin reduced ROS accumulation in $CDO1^{WT}$-overexpressing MKN45 (left) and NCI-N87 (right) cells compared to vehicle-treated controls. **g.** Engeletin also restored ATP production in $CDO1^{WT}$-expressing MKN45 (left) and NCI-N87 (right) cells. **h.** CCK-8 assays showed that engeletin partially rescued the proliferation of GC cells inhibited by $CDO1^{WT}$ (upper panel: MKN45; lower panel: NCI-N87). *$p < 0.05$, **$p < 0.01$, ***$p < 0.001$.

To assess whether the growth-inhibitory effect of CDO1 was primarily due to oxidative stress, N-acetylcysteine (NAC) was applied to alleviate ROS. However, neither proliferation nor ATP production was restored in NAC-treated GC cells compared with vehicle controls (**Figures 2a and 2b**). Recognizing the multifactorial nature of oxidative stress, an HTS of an antioxidant compound library was performed to identify agents capable of mitigating CDO1-induced ROS. Several compounds, including engeletin—a flavanonol glycoside derived from *Hymenaea martiana* with reported antioxidant properties [19, 20]—effectively reduced ROS, restored ATP levels, and improved viability in CDO1-overexpressing cells (**Figures 4e–h**). These results indicate that CDO1 suppresses GC cell proliferation in part by inducing oxidative stress.

CDO1-induced oxidative stress disrupts mitochondrial function

Oxidative stress can impair numerous cellular processes, particularly mitochondrial activity [21]. Measurement of mitochondrial membrane potential using JC-1 dye revealed that control GC cells exhibited predominantly red fluorescence (JC-1 aggregates), whereas CDO1-restored cells showed mostly green fluorescence (JC-1 monomers), indicative of mitochondrial depolarization (**Figure 5a**). Consistently, ATP production—a surrogate for mitochondrial function—was reduced by

approximately 50% in MKN45 and NCI-N87 cells expressing CDO1 (**Figure 5b**).

Seahorse extracellular flux analysis demonstrated that CDO1 strongly inhibited aerobic respiration, as reflected by decreases in both basal and maximal oxygen consumption rates (OCR) (**Figure 5c**). Additionally, CDO1 expression lowered glucose uptake and lactate secretion in both cell lines (**Figures 3a and 3b**). Targeted metabolomics further revealed that key energy and redox metabolites—including succinate, AMP, cis-aconitate, GMP, NADH, and NADPH—were significantly reduced in CDO1-overexpressing MKN45 cells (**Figure 5d**, **Table 3**). Of note, NADPH is critical for maintaining levels of reduced glutathione (GSH) and thioredoxins (TXN) [22], and its depletion further confirms that CDO1 exacerbates oxidative stress. Collectively, these findings indicate that CDO1-induced redox imbalance severely impairs mitochondrial function in GC cells.

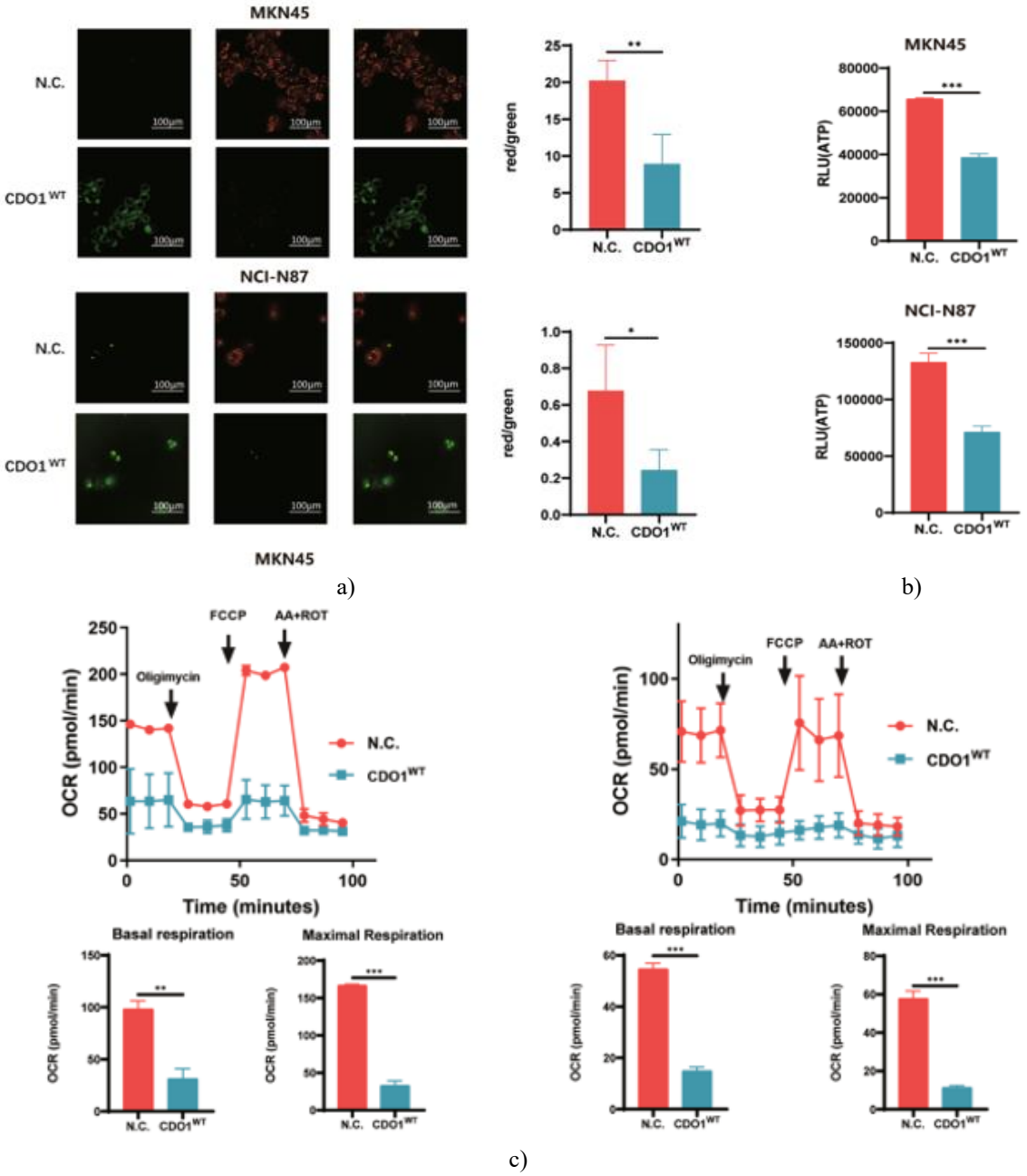

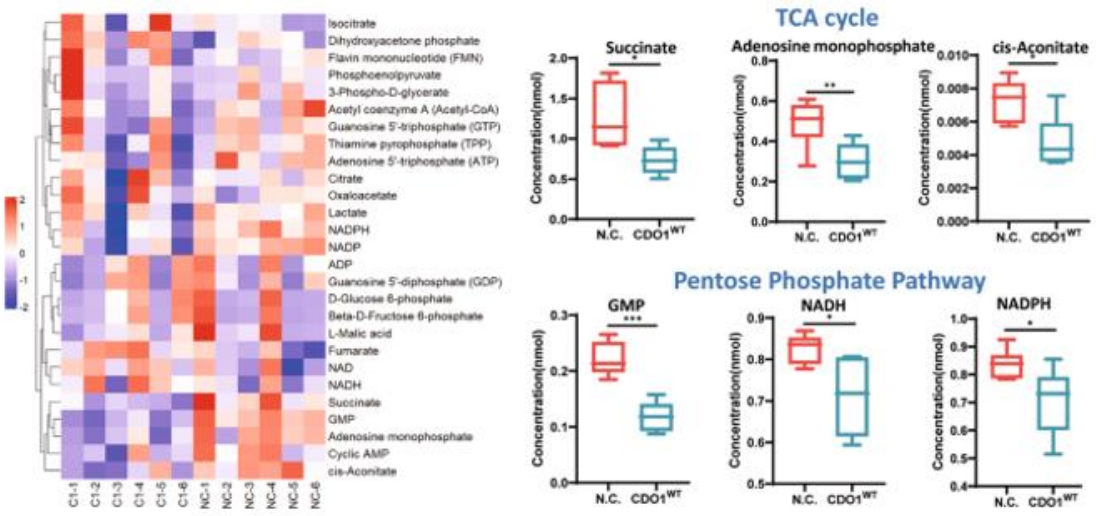

d)

Figure 5. Reintroduction of CDO1 disrupts mitochondrial activity in gastric cancer cell.

a. Mitochondrial membrane potential was evaluated using JC-1 staining as described in the Materials and Methods. Representative fluorescence images of control and CDO1-reconstituted MKN45 and NCI-N87 cells are shown (left). Quantitative analysis revealed a pronounced reduction in the red-to-green fluorescence ratio, reflecting mitochondrial depolarization following $CDO1^{WT}$ expression. Scale bars: 100 µm. **b.** Restoration of $CDO1^{WT}$ led to a marked decrease in intracellular ATP levels, indicating impaired mitochondrial energy production. **c.** Oxygen consumption rate (OCR) analysis demonstrated that $CDO1^{WT}$ significantly suppressed mitochondrial respiration in both MKN45 (left) and NCI-N87 (right) cells. Basal and maximal respiration rates were quantified below (mean ± SD; N = 3). Data shown are representative of two independent experiments. **d.** Targeted metabolomic profiling of ATP-related pathways revealed that levels of succinate, AMP, cis-aconitate, GMP, NADH, and NADPH were all significantly reduced in MKN45 cells expressing $CDO1^{WT}$ compared with control cells. *$p < 0.05$, **$p < 0.01$, ***$p < 0.001$.

CDO1-induced oxidative stress activates the integrated stress response in GC cells

The integrated stress response (ISR) is a conserved adaptive pathway activated by multiple stressors, including oxidative imbalance [23]. To determine whether CDO1 engages this pathway, we examined the expression of key ISR downstream genes. Overexpression of CDO1 resulted in a significant upregulation of ATF3, ATF4, TRIB3, and GADD34 mRNA levels in GC cells, whereas the enzymatically inactive CDO1 mutant had no such effect (**Figure 6a**). Consistent with ISR activation, increased nuclear localization of ATF4 and elevated phosphorylation of eIF2α at Ser51 were observed in CDO1^WT-expressing cells. Notably, treatment with engeletin attenuated both nuclear ATF4 accumulation and cytoplasmic phospho-eIF2α levels (**Figures 6b and c**). Since ISR signaling is initiated by four upstream kinases—HRI, PERK, PKR, and GCN2—that converge on eIF2α phosphorylation [23], we next evaluated their involvement. Selective depletion of HRI, but not PERK, PKR, or GCN2, restored proliferative capacity in GC cells expressing CDO1 (**Figure 6d**). Furthermore, loss of HRI markedly reduced ISR signaling triggered by CDO1, identifying HRI as the principal mediator of CDO1-induced ISR activation in this context (**Figure 6e**).

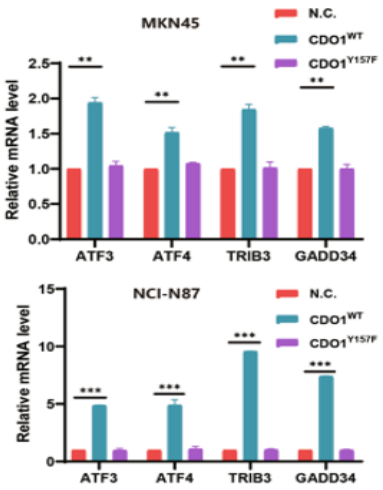

a)

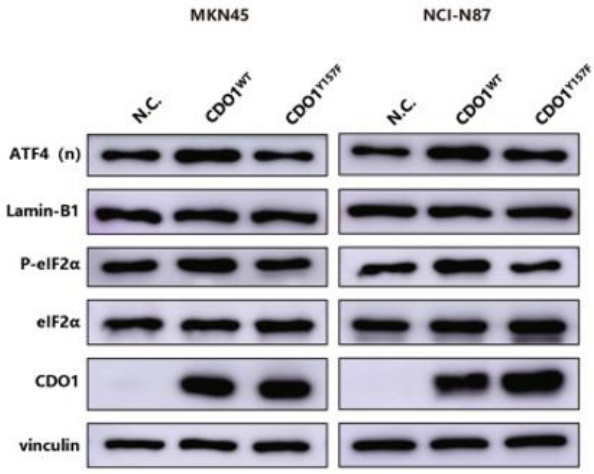

b)

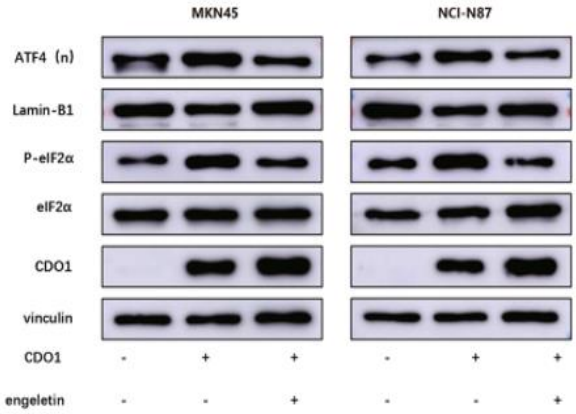

c)

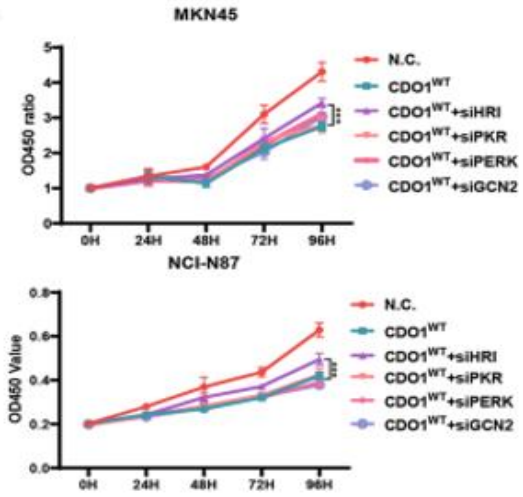

d)

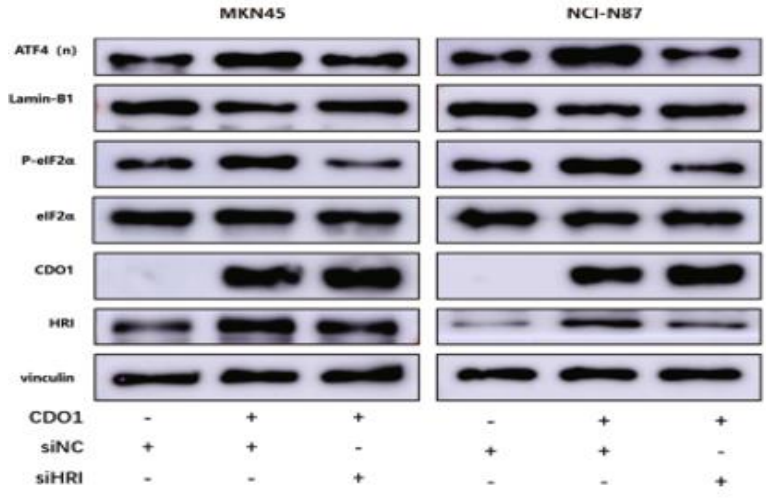

f)

Figure 6. Oxidative stress generated by CDO1 activates the integrated stress response

a. Quantitative PCR analysis of canonical ISR target genes revealed that wild-type CDO1 ($CDO1^{WT}$), but not the enzymatically inactive mutant $CDO1^{Y157F}$, significantly increased the transcript levels of ATF3, ATF4, TRIB3, and GADD34 in both MKN45 (top) and NCI-N87 (bottom) cells. **b.** Immunoblot analysis demonstrated enhanced nuclear accumulation of ATF4 and elevated cytoplasmic phosphorylation of eIF2α at Ser51 in MKN45 (left) and NCI-N87 (right) cells expressing $CDO1^{WT}$, whereas $CDO1^{Y157F}$ failed to induce these ISR markers. **c.** Treatment with the antioxidant engeletin markedly attenuated $CDO1^{WT}$-induced ISR activation, as evidenced by reduced nuclear ATF4 levels and diminished phosphorylation of eIF2α (Ser51) in both GC cell lines. **d.** Silencing of heme-regulated inhibitor kinase (HRI) significantly alleviated the proliferation block imposed by $CDO1^{WT}$ in MKN45 and NCI-N87 cells in vitro. **e.** Consistently, depletion of HRI reduced ISR signaling in $CDO1^{WT}$-expressing cells, as shown by decreased nuclear ATF4 and lower cytoplasmic phospho-eIF2α (Ser51) levels. Lamin B1 and vinculin were used as loading controls for nuclear and cytoplasmic fractions, respectively. $*p < 0.05$, $**p < 0.01$, $***p < 0.001$.

The growth-inhibitory effect of CDO1 requires activation of the ISR in gastric cancer cells

Given that CDO1 robustly activates the ISR in GC cells, we next evaluated whether this pathway mediates its cytostatic function. Pharmacological blockade of ISR signaling using ISRIB significantly restored ATP production in CDO1-overexpressing GC cells (**Figures. 7a and 7b**). Because phosphorylation of eIF2α at Ser51 is a central event in ISR activation, we ectopically expressed either wild-type eIF2α ($eIF2\alpha^{WT}$) or a non-phosphorylatable mutant ($eIF2\alpha^{S51A}$) in CDO1-restored MKN45 cells. Expression of $eIF2\alpha^{S51A}$ effectively suppressed ISR signaling and markedly increased ATP levels compared with $eIF2\alpha^{WT}$-expressing cells (**Figures 7c and 7d**).

In vivo, xenograft tumors derived from MKN45 cells co-expressing $CDO1^{WT}$ and $eIF2\alpha^{S51A}$ were substantially larger than those from cells expressing $CDO1^{WT}$ together with $eIF2\alpha^{WT}$ (**Figure. 7e**). Similarly, enforced expression of GADD34—an endogenous negative regulator of ISR—enhanced ATP production in $CDO1^{WT}$-expressing cells (**Figures. 7f and 7g**) and promoted tumor growth in mouse xenograft models (**Figure. 7h**).

Taken together, these results establish ISR activation as the principal mechanism through which CDO1 exerts its cytostatic effects in gastric cancer cells.

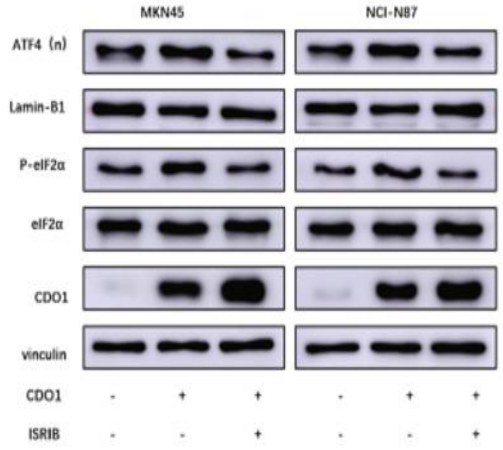

a)

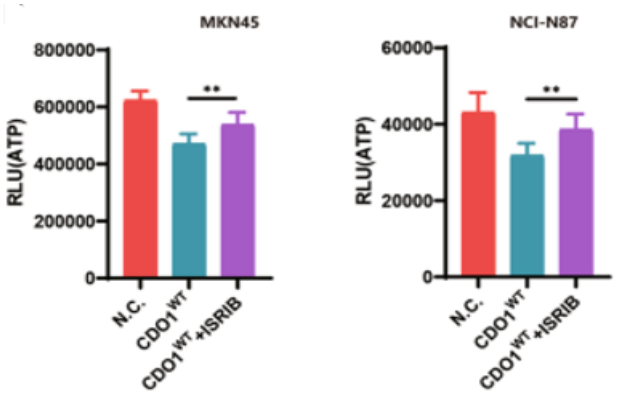

b)

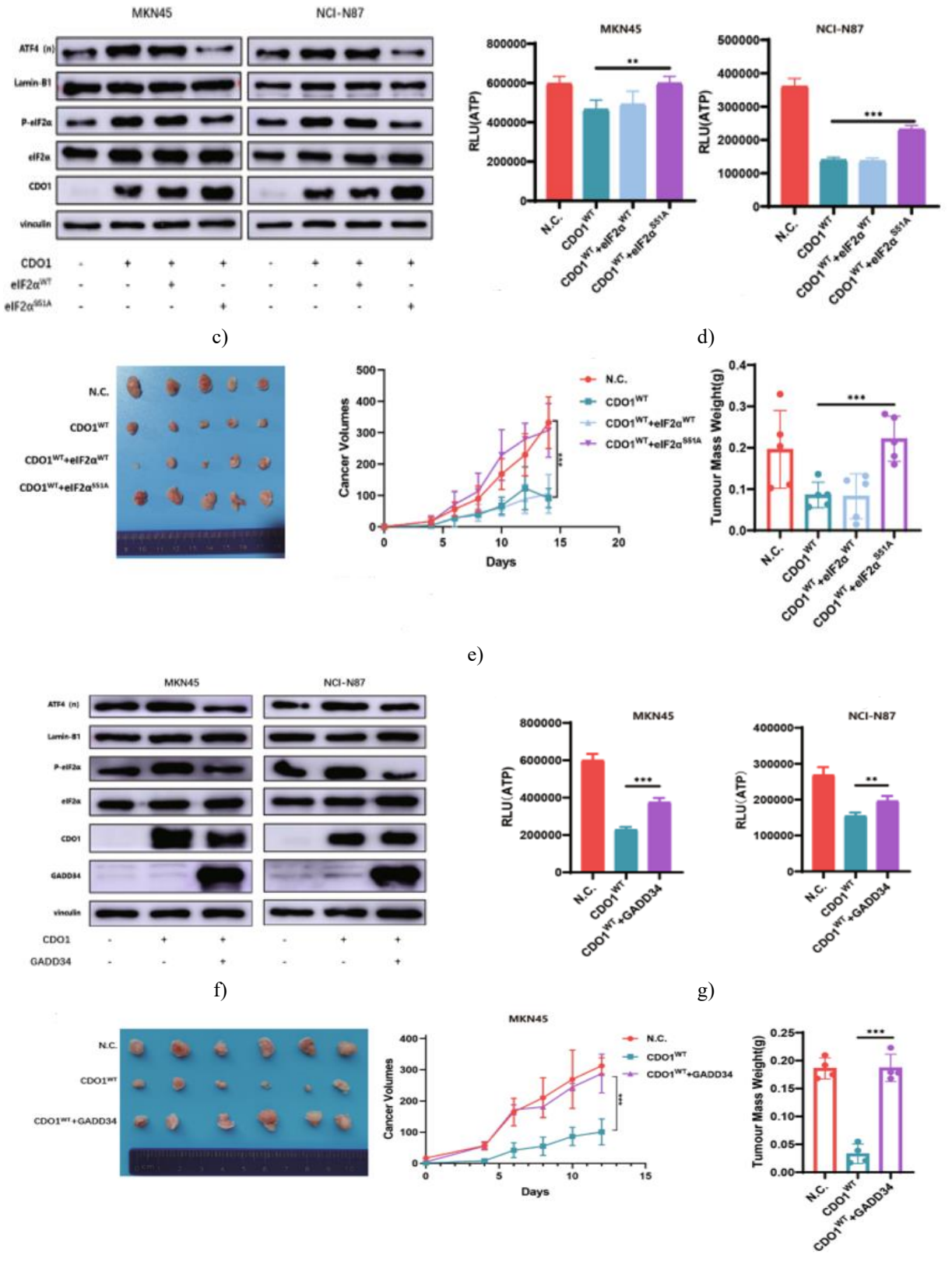

Figure 7. CDO1-mediated growth suppression in gastric cancer cells depends on ISR activation

a, b. Treatment with ISRIB, a pharmacological inhibitor of the integrated stress response, was applied to control and $CDO1^{WT}$-expressing GC cells. ISRIB effectively dampened ISR signaling, as evidenced by reduced nuclear ATF4 accumulation and decreased cytoplasmic phosphorylation of eIF2α at Ser51 **(a)**. Correspondingly, ATP levels were significantly elevated following ISRIB treatment in $CDO1^{WT}$-restored MKN45 (left) and NCI-N87 (right) cells **(b). C, d.** To genetically disrupt ISR signaling, Ser51 of eIF2α was substituted with alanine to generate a non-phosphorylatable mutant ($eIF2\alpha^{S51A}$). Compared with wild-type eIF2α, expression of $eIF2\alpha^{S51A}$ markedly suppressed ISR activation **(c)** and partially restored ATP production in $CDO1^{WT}$-expressing GC cells, as measured by luminescence assays **(d)**. Left panels: MKN45 cells; right panels: NCI-N87 cells. **e.** In a subcutaneous xenograft model, co-expression of $eIF2\alpha^{S51A}$ significantly alleviated the tumor growth inhibition imposed by $CDO1^{WT}$ in MKN45 cells implanted into Balb/c nude mice (N = 5 per group). **f, g.** Overexpression of GADD34 in CDO1-expressing MKN45 (left) and NCI-N87 (right) cells partially counteracted ISR activation **(f)** and increased intracellular ATP levels **(g). h.** Consistent with the in vitro findings, GADD34 expression substantially enhanced the in vivo growth of MKN45 xenograft tumors (N = 6 per group). Lamin B1 and vinculin served as loading controls for nuclear and cytoplasmic fractions, respectively. $^{**}p < 0.01$, $^{***}p < 0.001$.

Reduced expression of CDO1 has been observed across multiple cancer types, supporting its role as a tumor-suppressive factor. In non-small cell lung cancer (NSCLC), for instance, CDO1 is frequently silenced through promoter hypermethylation in tumors harboring KEAP1 mutations. This epigenetic repression protects cancer cells from oxidative injury by sustaining NRF2-driven antioxidant programs, whereas re-expression of CDO1 markedly compromises NSCLC cell viability by generating toxic sulfur-containing metabolites and depleting intracellular NADPH [18]. Consistent with these observations, our study demonstrates that CDO1 protein levels are significantly diminished in gastric cancer (GC) tissues and GC cell lines, and that restoring CDO1 expression strongly suppresses GC cell proliferation. Importantly, a catalytically inactive form of CDO1 failed to exert this inhibitory effect, indicating that its metabolic enzymatic activity is essential for its growth-suppressive function, similar to what has been reported in NSCLC.

Notably, GC cells appear to rely less on the NRF2/KEAP1 antioxidant axis, as GC incidence was not significantly increased in Nrf2-deficient mice compared with wild-type controls following benzo (a) pyrene exposure [24]. This observation prompted us to investigate alternative molecular pathways through which CDO1 constrains GC cell growth.

The role of oxidative stress in cancer is highly context-dependent, influenced by tumor type, stress intensity and duration, and the stage of tumor development [22]. Clinical evidence indicates that oxidative stress levels are significantly elevated in patients with GC and even in their first-degree relatives compared with individuals suffering from dyspepsia [25], suggesting that oxidative imbalance plays a crucial role in gastric carcinogenesis. Chronic *Helicobacter pylori* infection is a major contributor to sustained oxidative stress, which promotes malignant transformation through multiple mechanisms [26]. For example, *H. pylori*-induced oxidative stress increases histone H3 acetylation at the promoter of capping actin protein of muscle Z-line α subunit 1 (CAPZA1), leading to its upregulation [27]. CAPZA1, in turn, enhances the expression of CD44 and epithelial splicing regulatory protein 1 (ESRP1), with ESRP1 driving alternative splicing of CD44 to generate CD44 variant 9 (CD44v9), a marker of gastric cancer stem-like cells [27].

To tolerate persistently high oxidative stress while maintaining rapid proliferation, GC cells upregulate metabolic pathways that generate NADPH. Recent studies have shown that loss of key NADPH-producing enzymes—including nicotinamide nucleotide transhydrogenase (NNT), malic enzyme 1 (ME1), and diacylglycerol acyltransferase 2 (DGAT2)—leads to NADPH depletion, enhanced apoptosis, and reduced metastatic potential [28–30]. Collectively, these findings highlight the importance of tightly regulated redox homeostasis in GC initiation, progression, and dissemination.

In agreement with prior observations in NSCLC, re-expression of CDO1 in GC cells induced pronounced oxidative stress, as evidenced by increased ROS levels, reduced GSH/GSSG ratios, diminished NADPH availability, and compromised mitochondrial respiratory function. However, despite these changes, CDO1 did not trigger overt cell death pathways such as ferroptosis in GC cells **(Figure 5).** Interestingly, treatment with N-acetylcysteine (NAC), a well-established ROS scavenger, failed to rescue the cytostatic phenotype or

restore ATP production in CDO1-expressing GC cells. This may reflect the multifaceted effects of sulfite (SO_3^{2-}), a CDO1-generated metabolite that not only consumes cysteine through the formation of cysteine–sulfite adducts but may also exert broader regulatory effects within GC cells.

High-throughput screening of antioxidant compounds revealed that several agents, including engeletin, were capable of reversing CDO1-induced growth inhibition. Engeletin, a flavanonol glycoside known to suppress NF-κB signaling [31], significantly enhanced proliferation in GC cells with restored CDO1 expression. These results suggest that NF-κB–mediated antioxidant responses may be activated as a compensatory mechanism following CDO1 re-expression. The potential crosstalk between CDO1 activity and NF-κB signaling warrants further investigation.

To further elucidate how CDO1-driven redox imbalance leads to growth arrest, we focused on the integrated stress response (ISR), a conserved signaling pathway activated by oxidative stress that globally suppresses protein synthesis while selectively promoting the translation of stress-adaptive factors such as ATF4 [23]. Severe or prolonged stress conditions—for example, hyperosmotic stress—can induce translational arrest, ATP depletion, and ISR activation, enabling cells to resume proliferation once stress is alleviated [32]. Similarly, our data demonstrate that stable CDO1 expression activates the ISR through the HRI kinase, while engeletin mitigates both oxidative stress and ISR activation in GC cells.

Notably, ISR activation in this context strongly inhibited proliferation without inducing extensive cell death. Emerging evidence indicates that dysregulated ISR signaling in transformed cells or cancer-associated fibroblasts can facilitate tumor initiation and progression [33–35], thereby motivating therapeutic strategies aimed at modulating ISR activity [36]. Moreover, ISR activation via NF-κB signaling has been shown to promote the growth of endocrine therapy–resistant breast cancer cells [37]. Given the central role of NF-κB signaling in inflammation-driven gastric tumorigenesis [38, 39], whether NF-κB contributes to CDO1-induced ISR activation remains an important open question.

Several limitations of the present study should be acknowledged. First, CDO1 may exert context-dependent effects in GC, as ISR activation has been reported to confer resistance to cisplatin treatment [40], and our preliminary clinical observations suggest that higher CDO1 expression correlates with increased resistance to neoadjuvant SOX chemotherapy (data not shown). Since our study primarily examined established GC cell lines, the precise role of CDO1 in GC initiation and therapeutic response requires further investigation. Second, the mechanisms by which CDO1 dramatically elevates intracellular oxidative stress remain incompletely understood. Although sulfite-mediated disruption of glutathione synthesis likely contributes, the inability of NAC to reverse oxidative stress suggests the involvement of additional pathways. Third, we observed a discrepancy between our survival analysis based on CDO1 protein expression and results from the Kaplan–Meier Plotter database (www.kmplot.com). This inconsistency may stem from our direct assessment of CDO1 protein levels, which may more accurately reflect functional relevance than mRNA-based analyses. Supporting this notion, previous work has shown that increased CDO1 gene methylation independently predicts poor prognosis in GC patients [7]. Further studies are needed to reconcile these findings.

In summary, our data demonstrate that CDO1 suppresses GC cell proliferation both in vitro and in vivo through its enzymatic activity. Mechanistically, CDO1 induces oxidative stress, leading to activation of the integrated stress response and subsequent cytostasis. These findings highlight the tumor-suppressive role of CDO1 in gastric cancer and underscore its complex involvement in GC pathophysiology and therapeutic response, which merit deeper exploration.

Materials and Methods

Patient samples

Gastric carcinoma specimens together with paired adjacent non-malignant tissues were collected from 130 individuals who underwent radical gastrectomy at Tianjin Medical University Cancer Hospital (Tianjin, China) between January 2004 and September 2007. These samples were used for immunohistochemical evaluation of CDO1 protein expression. An additional cohort consisting of 30 matched GC and normal gastric tissues was obtained in 2021 at the same institution for analysis of CDO1 mRNA levels by quantitative PCR. None of the patients included in this study received preoperative chemotherapy or radiotherapy.

Culture conditions and cell lines

The human gastric cancer cell line NCI-N87 was purchased from the American Type Culture Collection

(ATCC, USA). MKN45 cells were kindly provided by Prof. Hui Li (Department of Gastrointestinal Cancer Biology, Tianjin Medical University Cancer Hospital and Institute, Tianjin, China). HEK-293T cells were a gift from Prof. Zhihua Liu (Cancer Hospital/ National Cancer Center, Beijing, China). Both MKN45 and NCI-N87 cells were maintained in RPMI-1640 medium supplemented with 10% fetal bovine serum (FBS), while HEK-293T cells were cultured under conditions recommended by ATCC. All experiments were performed using cells within 20 passages, and routine testing confirmed that all cell lines were free of mycoplasma contamination.

Chemical reagents and antibodies

Antibodies recognizing HRI (20582-1-AP), CDO1 (12589-1-AP), Lamin B1 (12987-1-AP) and GADD34 (10449-1-AP) were obtained from ProteinTech (Chicago, IL, USA). Antibodies against phosphorylated eIF2α (Ser51) (D9G8), total eIF2α (D7D3), and Vinculin (E1E9V) were purchased from Cell Signaling Technology (Danvers, MA, USA). An antibody targeting ATF4 (ab184909) was sourced from Abcam (Cambridge, UK).

Puromycin dihydrochloride (HY-B1743A), JC-1 mitochondrial dye (HY-15534), an antioxidant screening compound library (HY-L037), engeletin (HY-N0436), ISRIB (HY-12495), and Cell Counting Kit-8 (CCK-8; HY-K0301) were purchased from MedChemExpress. Stock solutions of engeletin (100 mM) and ISRIB (10 mM) were prepared in dimethyl sulfoxide (DMSO) according to the manufacturer's instructions. For cellular assays, engeletin and ISRIB were applied at final working concentrations of 5 μM and 10 μM, respectively.

Construction of plasmids, lentiviral packaging, and establishment of stable cell lines

The complete coding sequence of human CDO1 (designated $CDO1^{WT}$) was subcloned into the pLVX-IRES-puro lentiviral expression vector. To inactivate its catalytic activity, the tyrosine at position 157 was substituted with phenylalanine, creating the $CDO1^{Y157F}$ mutant [18]. Wild-type human eIF2α ($eIF2\alpha^{WT}$) was inserted into the pLVX-IRES-neo vector, and a serine-to-alanine mutation was made at residue 51 ($eIF2\alpha^{S51A}$) to block integrated stress response (ISR) signaling. Human GADD34 was similarly cloned into the pLVX-IRES-neo vector. Vectors lacking inserts (empty pLVX-IRES-puro or pLVX-IRES-neo) were included as negative controls (N.C.). To produce lentiviral particles, HEK-293T cells were co-transfected with the target pLVX constructs, the envelope plasmid pMD2.G (Addgene #12259), and the packaging plasmid psPAX2 (Addgene #12260). Lentiviral production and collection followed established protocols [41]. The gastric cancer cell lines NCI-N87 and MKN45 were transduced with the relevant viruses, followed by selection with puromycin and/or G418 to generate stable pools. Successful transgene expression was verified by Western blot analysis.

Small Interfering RNA (siRNA) knockdown and transfection

Target-specific siRNAs were custom-synthesized by RiboBio (Guangzhou, China).For each gene, a mixture of three independent siRNAs was transfected into NCI-N87 or MKN45 cells using Lipofectamine 2000 at a total concentration of 100 nM. A non-specific scramble siRNA (100 nM) served as the negative control (si-N.C.).

In vitro cell proliferation assays

Proliferative capacity was evaluated using the Cell Counting Kit-8 (CCK-8). Specifically, 1000 MKN45 or 3000 NCI-N87 cells were plated per well in 96-well plates with six replicates, and optical density at 450 nm was recorded on a BioTek plate reader at designated intervals. DNA replication was assessed via EdU incorporation with the Click-iT™ EdU Alexa Fluor™ 488 Flow Cytometry Assay Kit (Thermo Fisher Scientific) in MKN45 and NCI-N87 cells. For long-term growth assessment, 5×10^3 NCI-N87 cells from control or CDO1-expressing groups were seeded in 6-well plates and grown for ~10 days. Resulting colonies were fixed in methanol (15 min), stained with 0.5% crystal violet, and quantified under a microscope.

Quantification of Reactive Oxygen Species (ROS), ATP, and GSH/GSSG Ratio

Intracellular hydrogen peroxide was quantified with the ROS-Glo™ H_2O_2 Assay (Promega, Madison, WI, USA). Cellular ATP content was determined using the CellTiter-Glo Luminescent Cell Viability Assay (Promega). The ratio of reduced to oxidized glutathione (GSH/GSSG) was measured with the GSH/GSSG-Glo™ Assay (Promega). All assays were conducted per the manufacturer's guidelines, with luminescence read on a BioTek instrument at specified times.

Assessment of glucose consumption and lactate production in vitro

Glucose uptake from the medium and lactate release by control (N.C.) or CDO1-overexpressing MKN45 and NCI-N87 cells were measured using the Glucose Uptake-Glo™ and Lactate-Glo™ Assays (Promega), respectively, in accordance with the provided protocols.

rna isolation and quantitative reverse transcription PCR (RT-qPCR)

Total RNA from cell cultures or gastric cancer/normal tissues was purified using RNAiso Plus reagent (Takara Bio, Shiga, Japan). Reverse transcription was performed with the GoScript™ Reverse Transcription Kit (Promega). Quantitative PCR for CDO1 and other targets was carried out using TB Green Premix Ex Taq™ II (Takara Bio) on a QuantStudio 5 instrument (Applied Biosystems, Foster City, CA, USA), with GAPDH as the housekeeping gene. Tissue CDO1 levels were expressed via the −ΔCt approach, whereas fold changes in cell lines were calculated using the $2^{-\Delta\Delta}$Ct method.

Western blotting

Cells were lysed in buffer containing 10 mM Tris-HCl, 150 mM NaCl, 5 mM EDTA, 1% Triton X-100, and 0.25% sodium deoxycholate (pH 7.4), supplemented with protease/phosphatase inhibitors (Roche). Protein amounts were quantified with the Pierce™ BCA Assay (Thermo Fisher Scientific). Immunoblotting followed standard procedures previously detailed [41]. Signals were captured on an Amersham Imager 600 (GE Healthcare).

Immunofluorescence analysis

JC-1 dye was prepared as a 200 μM stock solution in DMSO. For fluorescence-based detection of mitochondrial membrane potential, MKN45 and NCI-N87 cells were plated into black-walled, clear-bottom 96-well plates (Corning, NY, USA). JC-1 was added directly to the culture medium to achieve a working concentration of 2 μM. After incubation for 15 min at 37 °C, cells were rinsed twice with PBS. Fluorescent images were captured using the Opera Phenix High-Content Screening System (PerkinElmer, Waltham, MA, USA). Quantification of mitochondrial polarization was performed by calculating the ratio of red (aggregated) to green (monomeric) fluorescence using Harmony® high-content analysis software (PerkinElmer).

Immunohistochemical staining

Formalin-fixed, paraffin-embedded gastric cancer and matched non-tumorous tissue sections were subjected to immunohistochemical staining using an anti-CDO1 antibody (1:400 dilution) following previously established protocols [41]. The proportion of positively stained cells and staining intensity were evaluated independently. These parameters were combined to generate a final IHC score. Cytoplasmic CDO1 expression was quantified based on the average staining intensity observed in tumor cells.

Targeted metabolomic profiling

Control and CDO1-reconstituted MKN45 cells were seeded in 10-cm culture dishes and harvested after 24 h using cell scrapers. Cell pellets were immediately snap-frozen in liquid nitrogen and stored at −80 °C until analysis. Quantitative targeted metabolomics focusing on 32 metabolites associated with cellular energy metabolism **(Table 3)** was conducted by Applied Protein Technology (Shanghai, China) using liquid chromatography–tandem mass spectrometry (LC–MS). Briefly, frozen samples were extracted in methanol:acetonitrile:H_2O (2:2:1, v/v), vortexed thoroughly, sonicated for 4 min, and incubated at −20 °C for 1 h to precipitate proteins. After centrifugation, supernatants were analyzed using an Agilent 1260 HPLC system coupled to an Agilent 6460 triple quadrupole mass spectrometer. The aqueous mobile phase consisted of H_2O containing 25 mM ammonium acetate and 25 mM ammonia (pH 9.75), while acetonitrile served as the organic phase. Instrument settings included a sheath gas temperature of 350 °C, dry gas temperature of 350 °C, sheath gas flow of 11 L/min, dry gas flow of 10 L/min, nebulizer pressure of 30 psi, nozzle voltage of 500 V, and capillary voltage of 4,000 V or −3,500 V for positive and negative ionization modes, respectively. Each MRM transition was monitored with a dwell time of 3 ms, yielding a total cycle time of 1.263 s. Data processing was carried out using MRMAnalyzer software.

High-throughput antioxidant screening

A curated antioxidant compound library comprising 778 small molecules was applied to identify agents capable of counteracting CDO1-induced oxidative stress. MKN45 cells stably expressing CDO1 were seeded into white 96-well plates (Corning) and allowed to attach for 24 h, reaching approximately 50% confluence. Compounds were dispensed using an Explorer G3 automated

workstation (PerkinElmer) and incubated for an additional 24 h at 37 °C in a humidified incubator with 5% CO_2. Each compound was tested at a final concentration of 5 μM, while DMSO-treated cells served as vehicle controls.

Cellular ATP content, used as a proxy for cell viability, was measured using the CellTiter-Glo luminescent assay (Promega) on an EnVision microplate reader configured for HTS applications (PerkinElmer). Luminescence values were normalized to vehicle controls, and relative changes were visualized as heatmaps. Fold changes were calculated according to the following formula: Fold change = (Reads (^{antioxidant}) − Reads (^{Vehicle})) / Reads (^{Vehicle}).

Tumor xenograft experiments

Female Balb/c nude mice (5 weeks old) were obtained from Vital River Laboratories (Beijing, China) and maintained under SPF conditions. For subcutaneous tumor formation assays, 5.0×10^5 MKN45 cells or 1.5×10^6 NCI-N87 cells from the designated experimental groups were injected into the flanks of the mice. Tumor dimensions were recorded every three days, and volumes were calculated using the equation: V = length × width² × 0.5. Animals were euthanized 20 days post-implantation, after which tumors were excised and weighed.

Statistical evaluation

With the exception of animal studies, immunohistochemical analyses, and high-throughput screening experiments, all assays were independently repeated at least twice. Quantitative data are presented as mean ± standard deviation. Statistical analyses were conducted using GraphPad Prism version 8 (San Diego, CA, USA). Comparisons between groups were performed using Student's *t*-test or χ^2-test, as appropriate. A *p* value below 0.05 was considered statistically significant. Significance thresholds were defined as *p < 0.05, **p < 0.01, and ***p < 0.001.

Acknowledgments: We would like to thank to Prof. Zhihua Liu (National Cancer Center/Cancer Hospital, Beijing, China) and Prof. Hui Li (Tianjin Medical University Cancer Institute and Hospital, Tianjin, China) for providing the cell lines used in this study. This work was supported by Tianjin Key Medical Discipline (Specialty) Construction Project (TJYXZDXK-009A), National Natural Science Foundation of China (81974373), and National Key R&D Program of China (Grant No. 2016YFC1303200).

Conflict of Interest: None

Financial Support: None

Ethics Statement: None

References

1. Diaz-Lagares A, Mendez-Gonzalez J, Hervas D, Saigi M, Pajares MJ, Garcia D, et al. A novel epigenetic signature for early diagnosis in lung cancer. Clin Cancer Res. 2016;22:3361–71.
2. Huang RL, Su PH, Liao YP, Wu TI, Hsu YT, et al. Integrated epigenomics analysis reveals a DNA methylation panel for endometrial cancer detection using cervical scrapings. Clin Cancer Res. 2017;23:263–72.
3. Jeschke J, O'Hagan HM, Zhang W, Vatapalli R, Calmon MF, Danilova L, et al. Frequent inactivation of cysteine dioxygenase type 1 contributes to survival of breast cancer cells and resistance to anthracyclines. Clin Cancer Res. 2013;19:3201–11.
4. Meller S, Zipfel L, Gevensleben H, Dietrich J, Ellinger J, Majores M, et al. CDO1 promoter methylation is associated with gene silencing and is a prognostic biomarker for biochemical recurrence-free survival in prostate cancer patients. Epigenetics. 2016;11:871–80.
5. Deckers IA, Schouten LJ, Van Neste L, van Vlodrop IJ, Soetekouw PM, et al. Promoter methylation of CDO1 identifies clear-cell renal cell cancer patients with poor survival outcome. Clin Cancer Res. 2015;21:3492–500.
6. Vedeld HM, Andresen K, Eilertsen IA, Nesbakken A, Seruca R, Gladhaug IP, et al. The novel colorectal cancer biomarkers CDO1, ZSCAN18 and ZNF331 are frequently methylated across gastrointestinal cancers. Int J Cancer. 2015;136:844–53.
7. Harada H, Hosoda K, Moriya H, Mieno H, Ema A, Ushiku H, et al. Cancer-specific promoter DNA methylation of Cysteine dioxygenase type 1 (CDO1) gene as an important prognostic biomarker of gastric cancer. PLoS One. 2019;14:e0214872.
8. Ooki A, Maleki Z, Tsay JJ, Goparaju C, Brait M, Turaga N, et al. A panel of novel detection and prognostic methylated DNA markers in primary

non-small cell lung cancer and serum DNA. Clin Cancer Res. 2017;23:7141–52.
9. Minatani N, Waraya M, Yamashita K, Kikuchi M, Ushiku H, Kojo K, et al. Prognostic significance of promoter DNA hypermethylation of cysteine dioxygenase 1 (CDO1) gene in primary breast cancer. PLoS One. 2016;11:e0144862.
10. Nakamoto S, Kumamoto Y, Igarashi K, Fujiyama Y, Nishizawa N, Ei S, et al. Methylated promoter DNA of CDO1 gene and preoperative serum CA19-9 are prognostic biomarkers in primary extrahepatic cholangiocarcinoma. PLoS One. 2018;13:e0205864.
11. Ushiku H, Yamashita K, Ema A, Minatani N, Kikuchi M, Kojo K, et al. DNA diagnosis of peritoneal fluid cytology test by CDO1 promoter DNA hypermethylation in gastric cancer. Gastric Cancer. 2017;20:784–92.
12. Harada H, Soeno T, Nishizawa N, Washio M, Sakuraya M, Ushiku H, et al. Prospective study to validate the clinical utility of DNA diagnosis of peritoneal fluid cytology test in gastric cancer. Cancer Sci. 2021;112:1644–54.
13. Sung H, Ferlay J, Siegel RL, Laversanne M, Soerjomataram I, Jemal A, et al. Global Cancer Statistics 2020: GLOBOCAN Estimates of Incidence and Mortality Worldwide for 36 Cancers in 185 Countries. CA Cancer J Clin. 2021;71:209–49.
14. Brait M, Ling S, Nagpal JK, Chang X, Park HL, Lee J, et al. Cysteine dioxygenase 1 is a tumor suppressor gene silenced by promoter methylation in multiple human cancers. PLoS One. 2012;7:e44951.
15. Ueki I, Roman HB, Valli A, Fieselmann K, Lam J, Peters R, et al. Knockout of the murine cysteine dioxygenase gene results in severe impairment in ability to synthesize taurine and an increased catabolism of cysteine to hydrogen sulfide. Am J Physiol Endocrinol Metab. 2011;301:E668–684.
16. Yu M, Gai C, Li Z, Ding D, Zheng J, Zhang W, et al. Targeted exosome-encapsulated erastin induced ferroptosis in triple negative breast cancer cells. Cancer Sci. 2019;110:3173–82.
17. Hao S, Yu J, He W, Huang Q, Zhao Y, Liang B, et al. Cysteine dioxygenase 1 mediates erastin-induced ferroptosis in human gastric cancer cells. Neoplasia. 2017;19:1022–32.
18. Kang YP, Torrente L, Falzone A, Elkins CM, Liu M, Asara JM, et al. Cysteine dioxygenase 1 is a metabolic liability for non-small cell lung cancer. Elife. 2019;8:e45572.
19. Pan C, Li B, Simon MC. Moonlighting functions of metabolic enzymes and metabolites in cancer. Mol Cell. 2021;81:3760–74.
20. Zhao X, Chen R, Shi Y, Zhang X, Tian C, Xia D. Antioxidant and anti-inflammatory activities of six flavonoids from Smilax glabra Roxb. Molecules. 2020;25:5295.
21. Sies H, Berndt C, Jones DP. Oxidative stress. Annu Rev Biochem. 2017;86:715–48.
22. Hayes JD, Dinkova-Kostova AT, Tew KD. Oxidative stress in cancer. Cancer Cell. 2020;38:167–97.
23. Costa-Mattioli M, Walter P. The integrated stress response: from mechanism to disease. Science. 2020;368:eaat5314.
24. Ramos-Gomez M, Kwak MK, Dolan PM, Itoh K, Yamamoto M, Talalay P, et al. Sensitivity to carcinogenesis is increased and chemoprotective efficacy of enzyme inducers is lost in nrf2 transcription factor-deficient mice. Proc Natl Acad Sci USA. 2001;98:3410–5.
25. Braga-Neto MB, Costa DVS, Queiroz DMM, Maciel FS, de Oliveira MS, Viana-Junior AB, et al. Increased oxidative stress in gastric cancer patients and their first-degree relatives: a prospective study from northeastern Brazil. Oxid Med Cell Longev. 2021;2021:6657434.
26. Butcher LD, den Hartog G, Ernst PB, Crowe SE. Oxidative stress resulting from helicobacter pylori infection contributes to gastric carcinogenesis. Cell Mol Gastroenterol Hepatol. 2017;3:316–22.
27. Tsugawa H, Kato C, Mori H, Matsuzaki J, Kameyama K, Saya H, et al. Cancer stem-cell marker CD44v9-positive cells arise from helicobacter pylori-Infected CAPZA1-overexpressing cells. Cell Mol Gastroenterol Hepatol. 2019;8:319–34.
28. Li S, Zhuang Z, Wu T, Lin JC, Liu ZX, Zhou LF, et al. Nicotinamide nucleotide transhydrogenase-mediated redox homeostasis promotes tumor growth and metastasis in gastric cancer. Redox Biol. 2018;18:246–55.
29. Lu YX, Ju HQ, Liu ZX, Chen DL, Wang Y, Zhao Q, et al. Correction: ME1 regulates NADPH homeostasis to promote gastric cancer growth and metastasis. Cancer Res. 2019;79:3789.

30. Li S, Wu T, Lu YX, Wang JX, Yu FH, Yang MZ, et al. Obesity promotes gastric cancer metastasis via diacylglycerol acyltransferase 2-dependent lipid droplets accumulation and redox homeostasis. Redox Biol. 2020;36:101596.
31. Wu H, Zhao G, Jiang K, Li C, Qiu C, Deng G. Engeletin alleviates lipopolysaccharide-induced endometritis in mice by inhibiting TLR4-mediated NF-kappaB activation. J Agric Food Chem. 2016;64:6171–8.
32. Jobava R, Mao Y, Guan BJ, Hu D, Krokowski D, Chen CW, et al. Adaptive translational pausing is a hallmark of the cellular response to severe environmental stress. Mol Cell. 2021;81:4191–4208.e4198.
33. Ghaddar N, Wang S, Woodvine B, Krishnamoorthy J, van Hoef V, Darini C, et al. The integrated stress response is tumorigenic and constitutes a therapeutic liability in KRAS-driven lung cancer. Nat Commun. 2021;12:4651.
34. Suresh S, Chen B, Zhu J, Golden RJ, Lu C, Evers BM, et al. eIF5B drives integrated stress response-dependent translation of PD-L1 in lung cancer. Nat Cancer. 2020;1:533–45.
35. Verginadis II, Avgousti H, Monslow J, Skoufos G, Chinga F, Kim K, et al. A stromal integrated stress response activates perivascular cancer-associated fibroblasts to drive angiogenesis and tumour progression. Nat Cell Biol. 2022;24:940–53.
36. Tian X, Zhang S, Zhou L, Seyhan AA, Hernandez Borrero L, Zhang Y, et al. Targeting the integrated stress response in cancer therapy. Front Pharm. 2021;12:747837.
37. Semina SE, Pal P, Kansara NS, Huggins RJ, Alarid ET, Greene GL, et al. Selective pressure of endocrine therapy activates the integrated stress response through NFkappaB signaling in a subpopulation of ER positive breast cancer cells. Breast Cancer Res. 2022;24:19.
38. Soutto M, Belkhiri A, Piazuelo MB, Schneider BG, Peng D, Jiang A, et al. Loss of TFF1 is associated with activation of NF-kappaB-mediated inflammation and gastric neoplasia in mice and humans. J Clin Invest. 2011;121:1753–67.
39. Cao L, Zhu S, Lu H, Soutto M, Bhat N, Chen Z, et al. Helicobacter pylori-induced RASAL2 through activation of nuclear factor-kappaB promotes gastric tumorigenesis via beta-catenin signaling axis. Gastroenterology. 2022;162:1716–31.e1717.
40. Wang SF, Wung CH, Chen MS, Chen CF, Yin PH, Yeh TS, et al. Activated integrated stress response induced by salubrinal promotes Cisplatin resistance in human gastric cancer cells via enhanced xCT expression and glutathione biosynthesis. Int J Mol Sci. 2018;19:3389.
41. Ma G, Jing C, Li L, Huang F, Ding F.Wang B, et al. MicroRNA-92b represses invasion-metastasis cascade of esophageal squamous cell carcinoma. Oncotarget. 2016;7:20209–22.